TABLE 3. The specificity and sensitivity of ELISAs and comparison of ELISA and IFAT results

Parameter	BbMSA	BbRAP-1CT	BbTRAP-T	BbSBP-1	BbSBP-4
Specificity (%)	85.3	72.3	54.85	91.49	96.01
Sensitivity (%)	83.95	64.2	23.45	91.35	96.43
Concordance (%)	72.9	66.53	56.5	76.33	85.3
Kappa value	0.461	0.339	0.153	0.528	0.705

cordance) between the IFAT and the ELISA was calculated to be 56.5% (rBbTRAP-T), 66.53% (rBbRAP-1CT), 72.9% (rBbMSA-2c), 76.33% (rBbSBP-1), and 85.3% (rBbSBP-4), and the kappa values were determined to be 0.153, 0.339, 0.461, 0.528, and 0.705, respectively (Table 3). These results revealed that rBbSBP-4 is the best diagnostic antigen assayed in the ELISA for the detection of a specific antibody to *B. bovis* among five antigens examined.

DISCUSSION

The global impact of bovine babesiosis has spurred an interest in developing effective diagnostic strategies that could lead to better management of the control of infection. *B. bovis* infection can be diagnosed directly by microscopic examination or PCR and indirectly with several serological methods (31). Although all of these tests have shortcomings, the serological tests, particularly the ELISA, seems to be the most practical and economical for epidemiological investigation (2, 7, 8). Indeed, the ELISA offers greater sensitivity, objectivity, and capacity for quick adaptation to test a large number of sera than any of the existing serological tests. The crude antigen prepared from merozoites has been utilized traditionally for serological detection; however, recombinant protein can be an alternative source, allowing better standardization of the test while reducing the cost of the massive production of the parasite (7, 9, 21). At this point, many recombinant antigens have been evaluated for diagnostic ELISAs; however, their sensitivities in diverse geographic areas have not produced perfect results. Therefore, further research on new antigens is extremely desirable for the development of a standard global assay. Within this context, we have validated five ELISAs utilizing deferent recombinant proteins and evaluated their usefulness for global application.

Although the ELISAs based on recombinant proteins differentiated clearly between experimentally *B. bovis*-infected and other closely related protozoan-infected bovine sera, their performances using field bovine sera varied, especially in comparison to IFAT results. Of note, rBbSBP-4 demonstrated the best performance, with high specificity, sensitivity, and agreement rates with the IFAT. These might be due to the fact that BbSBP-4 is a unique protein that has no significant homology with other apicomplexan parasites and is highly conserved among different geographic isolates from Asia, Africa, and South America (Terkawi et al., submitted). In addition, BbSBP-4 was found to shed within the cytoplasm of infected RBC in the late developmental stage of the parasites and was, subsequently, detected as an exoantigen in the supernatant of an *in vitro* culture (Terkawi et al., submitted). The secretion nature of BbSBP-4 may make the molecule very immunogenic during infection and allow direct interaction with host immune cells. On the other hand, rBbSBP-1 showed good diagnostic performance, with promising specificity and sensitivity for the detection of infection. Indeed, BbSBP-1 has been documented to be an immunodominant 80-kDa merozoite protein located in the spherical bodies, detected within the cytoplasmic face of the infected RBC membrane shortly after the invasion, and capable of eliciting the proliferation of both $CD4^+$ and $CD8^+$ T lymphocytes (16, 27). The better performance of rBbSBP-4 than of rBbSBP-1 in diagnosis might be due to the characteristics of the native protein which is found abundantly in the cytosol of infected host cells in the late stage of division of the parasites and, consequently, in the supernatant of the culture (Terkawi et al., submitted). This allows a direct and longer exposure to host immune cells (17). Moreover, the analyses of the determinant's composition based on an *in silico* epitope are necessary to understand antigenic attributes of these molecules. Further study including the combination of the two antigens on the basis of their B- and T-cell epitopes in the ELISA might be valuable, providing more accurate diagnostic tools for the detection of *B. bovis* infection.

A major membrane protein, BbMSA-2c, is a member of the complex VMSA genes and is known as a promising diagnostic antigen (19). Members of this family, however, exhibit high sequence variability among geographically distant strains (23). This might be the reason for the lower antigenicity of rBbMSA-2c for the detection of infection and might limit its potential for global diagnosis. The rhoptry-associated protein 1 (RAP-1) occurs in all *Babesia* species, has significant sequence homology with other apical complex proteins, and includes neutralization-sensitive B-cell and T-cell epitopes (24). BbRAP-1 is known as an exoantigen that is detected within the cytoplasm of infected RBC at the early stage of infection and persists shortly before disappearing at the ring stage (26, 27, 33). The full-length protein has been documented to be unsuitable for diagnosis due to the high conservation of 300 amino acids at the N-terminal region, which causes cross-reactivity with other *Babesia* spp. On the contrary, the C terminus presents distinct sequences with low identities with other *Babesia* RAP-1s and can serve as a species-specific diagnostic antigen (5, 6, 26). Therefore, the C terminus of BbRAP-1 has been used broadly as an antigen for serodiagnosis and epidemiological surveys, with high reliability (6, 18). However, our data have shown that this antigen had good performance with samples from Asia but not with those from Ghana and Brazil. In support of this, Boonchit et al. (5) have noted that rBbRAP-1CT has better performance for the detection of infection in Mongolian than Brazilian serum samples. The low sensitivity of rBbRAP-1CT is probably due to diversity in the sequences encoding the C-terminal region among geographically distant strains. Unexpectedly, rBbTRAP-T showed the lowest specificity and sensitivity with field serum samples, indicating that this antigen is not suitable for the development of a serological test. In a related study, rBgTRAP was noted as the best antigen for the detection of infection with *B. gibsoni* in canine sera (14, 26). The discrepancies in performance might be due to differences in the host and immune responses as well as the low identical homology between the genes in the species.

Serological diagnosis of *Babesia* infection is usually based on the detection of the antibodies against asexual blood-stage parasites. Although the IFAT has been a reliable serological

test in recent decades, it is time-consuming and subjective. Additionally, it cannot be automated, and results are largely influenced by the degree of training of the technician. Recently, the competitive ELISA (cELISA) with the C terminus of the rhoptry-associated protein 1 has been validated and undergone interlaboratory validation under OIE standards (12, 13). Despite the high specificity and sensitivity of the cELISA with *B. bovis*-infected sera from different geographic regions, the assay has shown a limitation in detecting the early stage of infection. Indeed, the IFAT could detect specific antibodies in experimentally *B. bovis*-infected sera about 2 days before the cELISA (12). Moreover, Goff et al. (13) have noted that samples with low OD values (near the cutoff point) in the cELISA should be repeated for further confirmation. These may affect the accuracy of the diagnosis in epidemiological investigation, particularly with carrier animals that have low antibody titers. Therefore, there is a need to continue research on the development of effective diagnostic assays. In the present study, we attempted to develop an indirect ELISA for the diagnosis of *B. bovis* infection. Our results demonstrated the usefulness of an ELISA utilizing rBbSBP-4 for the serological detection of *B. bovis* infection in cattle from different geographic regions of the world. The ELISA with rBbSBP-4 provides a more practical and sensitive tool than the standard IFAT and thus will be applicable for epidemiological surveys and control of the disease. Further investigations including a direct comparison of this ELISA with the previously validated cELISA (13) are required to achieve better diagnosis of *B. bovis* infection in the future.

ACKNOWLEDGMENTS

This work was supported by a grant from the Global COE Program (J02) and a Grant-in-Aid for Scientific Research (B-19405044), both from the Ministry of Education, Culture, Sports, Science, and Technology, Japan, and a program for the Promotion of Basic Research Activities for Innovative Bioscience (PROBRAIN).

M.A.T. was supported by a research grant fellowship from the Japanese Society for the Promotion of Science (JSPS) for young scientists. N.X.H., P.E.W., and F.J.S. were supported by Japan International Cooperation Agency (JICA).

REFERENCES

1. **Altangerel, K., et al.** 2009. Evaluation of *Babesia bigemina* 200 kDa recombinant antigen in enzyme-linked immunosorbent assay. Parasitol. Res. **105:** 249–254.
2. **Araújo, F. R., et al.** 1998. Comparison between enzyme-linked immunosorbent assay, indirect fluorescent antibody and rapid conglutination test in detecting antibodies against *Babesia bovis*. Vet. Parasitol. **74:**101–108.
3. **Bock, R., L. Jackson, A. de Vos, and W. Jorgensen.** 2004. Babesiosis of cattle. Parasitology **129:**247–269.
4. **Bono, M. F., et al.** 2008. Efficiency of a recombinant MSA-2c-based ELISA to establish the persistence of antibodies in cattle vaccinated with *Babesia bovis*. Vet. Parasitol. **157:**203–210.
5. **Boonchit, S., et al.** 2002. Evaluation of an enzyme-linked immunosorbent assay with recombinant rhoptry-associated protein-1 antigen of *Babesia bovis* for the detection of specific antibodies in cattle. J. Clin. Microbiol. **40:**3771–3775.
6. **Boonchit, S., et al.** 2004. Improved enzyme-linked immunosorbent assay using C-terminal truncated recombinant antigens of *Babesia bovis* rhoptry-associated protein-1 for detection of specific antibodies in cattle. J. Clin. Microbiol. **42:**1601–1604.
7. **Böse, R., R. H. Jacobson, K. R. Gale, D. J. Waltisbuhl, and I. G. Wright.** 1990. An improved ELISA for detection of antibodies against *Babesia bovis* using either a native or a recombinant *B. bovis* antigen. Parasitol. Res. **76:**648–652.
8. **Böse, R., W. K. Jorgensen, R. J. Dalgliesh, K. T. Friedhoff, and A. J. de Vos.** 1995. Current state and future trends in diagnosis of babesiosis. Vet. Parasitol. **57:**61–74.
9. **de Echaide, S. T., et al.** 1995. Evaluation of enzyme-linked immunosorbent assay kit to detect *Babesia bovis* antibodies in cattle. Prev. Vet. Med. **24:**277–283.
10. **de Vos, A. J., and F. T. Potgieter.** 1994. Bovine babesiosis, p. 278–294. *In* J. A. W. Coetzer, G. R. Thomson, and R. C. Tustin (ed.), Infectious diseases of livestock. Oxford University Press, Cape Town, South Africa.
11. **Gaffar, F. R., A. P. Yatsuda, F. F. Franssen, and E. de Vries.** 2004. A *Babesia bovis* merozoite protein with a domain architecture highly similar to the thrombospondin-related anonymous protein (TRAP) present in *Plasmodium* sporozoites. Mol. Biochem. Parasitol. **136:**25–34.
12. **Goff, W. L., et al.** 2003. Competitive enzyme-linked immunosorbent assay based on a rhoptry-associated protein 1 epitope specifically identifies *Babesia bovis*-infected cattle. Clin. Diagn. Lab. Immunol. **10:**38–43.
13. **Goff, W. L., et al.** 2006. Validation of a competitive enzyme-linked immunosorbent assay for detection of antibodies against *Babesia bovis*. Clin. Vaccine Immunol. **13:**1212–1216.
14. **Goo, Y. K., et al.** 2008. *Babesia gibsoni*: serodiagnosis of infection in dogs by an enzyme-linked immunosorbent assay with recombinant BgTRAP. Exp. Parasitol. **118:**555–560.
15. **Hines, S. A., G. H. Palmer, D. P. Jasmer, T. C. McGuire, and T. F. McElwain.** 1992. Neutralization-sensitive merozoite surface antigens of *Babesia bovis* encoded by members of a polymorphic gene family. Mol. Biochem. Parasitol. **55:**85–94.
16. **Hines, S. A., et al.** 1995. Genetic and antigenic characterization of *Babesia bovis* merozoite spherical body protein Bb-1. Mol. Biochem. Parasitol. **69:** 149–159.
17. **Homer, M. J., et al.** 2003. Identification and characterization of putative secreted antigens from *Babesia microti*. J. Clin. Microbiol. **41:**723–729.
18. **Iseki, H., et al.** 2010. Seroprevalence of *Babesia* infections of dairy cows in northern Thailand. Vet. Parasitol. **170:**193–196.
19. **Kim, C. M., et al.** 2008. Development of a rapid immunochromatographic test for simultaneous serodiagnosis of bovine babesiosis caused by *Babesia bovis* and *Babesia bigemina*. Am. J. Trop. Med. Hyg. **78:**117–121.
20. **Levy, M. G., and M. Ristic.** 1980. *Babesia bovis*: continuous cultivation in a microaerophilus stationary phase culture. Science **204:**1218–1220.
21. **Machado, R. Z., et al.** 1997. An enzyme-linked immunosorbent assay (ELISA) for the detection of antibodies against *Babesia bovis* in cattle. Vet. Parasitol. **71:**17–26.
22. **McCosker, P. J.** 1981. The global importance of babesiosis, p. 1–24. *In* M. Ristic and J. P. Kreier (ed.), Babesiosis. Academic Press, Inc., New York, NY.
23. **Palmer, G. H., et al.** 1991. Strain variation of *Babesia bovis* merozoite surface-exposed epitopes. Infect. Immun. **59:**3340–3342.
24. **Suarez, C. E., et al.** 1991. Characterization of the gene encoding a 60-kilodalton *Babesia bovis* merozoite protein with conserved and surface exposed epitopes. Mol. Biochem. Parasitol. **46:**45–52.
25. **Terkawi, M. A., et al.** 2007. *Babesia gibsoni* ribosomal phosphoprotein P0 induces cross-protective immunity against *B. microti* infection in mice. Vaccine **25:**2027–2035.
26. **Terkawi, M. A., et al.** 2009. Molecular characterizations of three distinct *Babesia gibsoni* rhoptry-associated protein-1s (RAP-1s). Parasitology **136:** 1147–1160.
27. **Tetzlaff, C. L., A. C. Rice-Ficht, V. M. Woods, and W. C. Brown.** 1992. Induction of proliferative responses of T cells from *Babesia bovis*-immune cattle with a recombinant 77-kilodalton merozoite protein (Bb-1). Infect. Immun. **60:**644–652.
28. **Uilenberg, G.** 2006. *Babesia*—a historical overview. Vet. Parasitol. **138:**3–10.
29. **Waltisbuhl, D. J., I. G. Goodger, I. G. Wright, M. A. Commins, and D. F. Mahoney.** 1987. An enzyme-linked immunosorbent assay to diagnose *Babesia bovis* infection in cattle. Parasitol. Res. **73:**126–131.
30. **Weiland, G., and I. Reiter.** 1988. Methods for serological response to *Babesia*, p. 143–158. *In* M. Ristic. (ed.), Babesiosis of domestic animals and man. CRC Press, Inc., Boca Raton, FL.
31. **World Organization for Animal Health (OIE).** 2008. Chapter 2.3.8, Bovine babesiosis. *In* Manual of diagnostic tests and vaccines for terrestrial animals. OIE, Paris, France. http://www.oie.int/fr/normes/mmanual/A_00059.htm.
32. **Xuan, X., et al.** 2001. Expression of *Babesia equi* merozoite antigen 1 in insect cells by a recombinant baculovirus and evaluation of its diagnostic potential in an enzyme-linked immunosorbent assay. J. Clin. Microbiol. **39:**705–709.
33. **Yokoyama, N., et al.** 2002. Cellular localization of *Babesia bovis* merozoite rhoptry-associated protein 1 and its erythrocyte-binding activity. Infect. Immun. **70:**5822–5826.
34. **Yokoyama, N., M. Okamura, and I. Igarashi.** 2006. Erythrocyte invasion by *Babesia* parasites: current advances in the elucidation of the molecular interactions between the protozoan ligands and host receptors in the invasion stage. Vet. Parasitol. **138:**22–32.

PROTIST, in press

Compartmentalization of a Glycolytic Enzyme in *Diplonema*, a Non-kinetoplastid Euglenozoan

Takashi Makiuchi[a,1], Takeshi Annoura[a,2], Muneaki Hashimoto[a], Tetsuo Hashimoto[b], Takashi Aoki[a], and Takeshi Nara[a,3].

[a]Department of Molecular and Cellular Parasitology, Juntendo University School of Medicine, 2-1-1 Hongo, Bunkyo-ku, Tokyo 113-8421, Japan
[b]Institute of Biological Sciences, University of Tsukuba, 1-1-1 Tennoudai, Tsukuba, Ibaraki 305-8572, Japan

Running title: Glycosome-like Organelles in Diplonemids

[1]Current address: Department of Parasitology, National Institute of Infectious Diseases, 1-23-1 Toyama, Shinjuku-ku, Tokyo 162-8640, Japan
[2]Current address: Leiden Malaria Research Group, Department of Parasitology, Centre for Infectious Diseases, Leiden University Medical Center, LUMC, L4-Q, Albinusdreef 2, 2333 ZA Leiden, Netherlands.
[3]Corresponding author; Fax +81 3 5800 0476
e-mail tnara@juntendo.ac.jp (T. Nara)

Abstract

Glycosomes are peroxisome-related organelles containing glycolytic enzymes that have been found only in kinetoplastids. We show here that a glycolytic enzyme is compartmentalized in diplonemids, the sister group of kinetoplastids. We found that, similar to kinetoplastid aldolases, the fructose 1,6-bisphosphate aldolase of *Diplonema papillatum* possesses a type 2-peroxisomal targeting signal. Western blotting showed that this aldolase was present predominantly in the membrane/organellar fraction. Immunofluorescence analysis showed that this aldolase had a scattered distribution in the cytosol, suggesting its compartmentalization. In contrast, orotidine-5'-monophosphate decarboxylase, a non-glycolytic glycosomal enzyme in kinetoplastids, was shown to be a cytosolic enzyme in *D. papillatum*. Since euglenoids, the earliest diverging branch of Euglenozoa, do not possess glycolytic compartments, these findings suggest that the routing of glycolytic enzymes into peroxisomes may have occurred in a common ancestor of diplonemids and kinetoplastids, followed by diversification of these newly established organelles in each of these euglenozoan lineages.

Key Words: Euglenozoa; evolution; glycosome; kinetoplastids; peroxisome; trypanosomatids.

Introduction

Peroxisomes are cellular compartments surrounded by a single membrane and present in almost all eukaryotes. These specialized organelles are involved in the oxidation of various organic substrates using molecular oxygen. This process results in the generation of toxic hydrogen peroxide, which must be

detoxified by catalase. Peroxisomes participate in important metabolic pathways, including the β-oxidation of fatty acids, free radical detoxification, and purine/pyrimidine degradation (Gabaldón et al. 2006; Parsons et al. 2001; Schlüter et al. 2006).

The physiological functions and enzymatic contents of peroxisomes vary across species and often among growth conditions (Michels et al. 2005; Parsons et al. 2001). For example, glyoxysomes, the specialized form of peroxisomes found in germinating plant seeds, contain enzymes of the glyoxylate cycle, whereas peroxisomes of leaves contain enzymes of the glycolate pathway, a difference regarded as a typical example of organellar diversification (Gabaldón 2010; Hayashi et al. 2000; Tolbert et al. 1968).

The protistan group Euglenozoa includes three major lineages, euglenoids, diplonemids, and kinetoplastids, with euglenoids constituting the earliest branch followed by the separation of the diplonemid and kinetoplastid lineages (Cavalier-Smith 1981; Simpson et al. 2002; Simpson and Roger 2004). Kinetoplastids consist of bodonids and trypanosomatids, the latter of which include medically important pathogens, such as *Trypanosoma brucei*, which causes sleeping sickness (African Trypanosomiasis); *T. cruzi*, which causes Chagas disease (American Trypanosomiasis) and *Leishmania* spp., which cause leishmaniasis.

The presence of peroxisomes in euglenoids is not fully understood. *Euglena* possesses peroxisome-like particles but lacks catalase activity (Collins and Merrett 1975; Graves et al. 1971; Shigeoka et al. 1980). In contrast, kinetoplastids possess unique peroxisome like-organelles, called glycosomes, characterized by compartmentalization of most of the glycolytic pathway (Michels et al. 2006; Opperdoes and Borst 1977; Opperdoes et al. 1988). In addition, glycosomes contain other metabolic enzymes, such as most of the enzymes of the purine salvage pathway and the last two enzymes of the de novo pyrimidine biosynthetic pathway, orotate phosphoribosyltransferase (OPRT) and orotidine-5'-monophosphate decarboxylase (OMPDC) (Hammond and Gutteridge 1982; Michels et al. 2000). These findings highlight the unique evolution of peroxisomes in the kinetoplastid lineage.

The evolutionary trail by which peroxisomes gave rise to glycosomes in kinetoplastids, however, remains unclear, due largely to the lack of biochemical and genetic information regarding the nature of peroxisomes and peroxisome-related organelles in diplonemids, the closest relatives of kinetoplastids. We previously reported that the structure of the *OPRT* and *OMPDC* genes varies among euglenozoan lineages (Makiuchi et al. 2007; Makiuchi et al. 2008). Euglenoids possess a *OMPDC-OPRT* fusion gene, with the OMPDC activity present in the cytosol (Walther et al. 1980). In contrast, kinetoplastids possess an inversely fused *OMPDC-OPRT* gene, with the OMPDC-OPRT fusion protein having a peroxisome-targeting signal (C-terminal PTS1), suggesting that it is localized in glycosomes. In the diplonemid, *Diplonema papillatum*, the subcellular localization of OMPDC (and putative OPRT) has not yet been determined. We found that *D. papillatum OMPDC* is a stand-alone gene, lacking the consensus sequence of a PTS, suggesting that the protein is localized in the cytosol (Makiuchi et al. 2008).

In the present study, we examined whether glycosome-associated enzymes are compartmentalized in diplonemids. We characterized two enzymes, the glycolytic fructose 1,6-bisphosphate aldolase (ALD) and OMPDC in *D. papillatum*. We demonstrate that a consensus sequence of an N-terminal PTS2 is present in ALD of *D. papillatum*, suggesting that this enzyme is localized in peroxisomes, as is that of trypanosomatids. Phylogenetic analysis showed monophyly of trypanosomatid and diplonemid ALDs. Biochemical analysis showed the different distributions of ALD and OMPDC, predominantly in the membrane-rich and cytosolic fractions, respectively. Immunofluorescence analysis showed that *D. papillatum* ALD has a scattered pattern of distribution, whereas OMPDC has a uniform pattern of distribution. Our findings may provide insights into the distinct evolution of peroxisome like-organelles in the different euglenozoan lineages.

Results

Presence of a Peroxisomal Targeting Signal in *D. papillatum* ALD

ALD is a glycosomal enzyme in trypanosomatids (Hart et al. 1984; Taylor and Gutteridge 1987). Full-length ALD cDNA of *D. papillatum* (GenBank™ AB550707) was cloned based on its partial sequence registered in the TBest database (http://tbestdb.bcm.umontreal.ca/searches/login.php). In general, ALDs can be divided into two

classes, Class I and Class II; Class I aldolases are present in vertebrates, plants and a number of protists and prokaryotes (see Fig. 2), whereas Class II aldolases are present in fungi, several protists and many prokaryotes (Rutter 1964). We found that the amino acid sequence of *D. papillatum* ALD showed identities of 63%, 45%, 48%, and 50% with the Class I ALDs of trypanosomatids, *Euglena gracilis* (euglenoids), *Arabidopsis thaliana* (plants), and humans (animals), respectively.

D. papillatum ALD is comprised of 374 amino acids and has an estimated molecular weight of 41 kD. The amino acid residues constituting the active site of class-I ALD are fully conserved in *D. papillatum* ALD (St-Jean et al. 2005). Indeed, recombinant *D. papillatum* ALD expressed in *Escherichia coli* was able to catalyze the formation of glyceraldehyde-3-phosphate and dihydroxyacetone phosphate from the substrate, fructose-1,6-bisphospate (data not shown). The most striking feature of *D. papillatum* ALD is the presence of a consensus N-terminal peroxisomal targeting signal (PTS2) present in trypanosomatid ALDs (Gabaldón 2010; Michels et al. 2005), suggesting that *D. papillatum* ALD is likely to localize in peroxisome-related compartments (Fig. 1A).

D. papillatum ALD Has a Common Evolutionary Origin as Glycosomal ALDs of Kinetoplastids

We examined whether the targeting of ALD to peroxisome-related organelles occurred in the common ancestor of diplonemids and kinetoplastids or evolved independently in each lineage. Phylogenetic analysis of Class I ALDs clearly showed monophyly of diplonemid and trypanosomatid ALDs within the eukaryotic clade with strong bootstrap support (Fig. 2). The evolutionary origin of euglenoid Class I ALD is unclear, due mainly to the lack of resolution. It is worth noting that euglenoids possess both Class I (plastid) and Class II (cytosolic) ALDs (Plaumann et al. 1997). The finding, that euglenoid Class I ALD did not fall into the diplonemid/kinetoplastid clade, suggests their different origin, the former originating probably from a secondary endosymbiont (an algal lineage) that gave rise to the plasmid. We conclude that the addition of PTS2 to ALD may have occurred in the common ancestor of diplonemids and kinetoplastids after separation of the euglenoid lineage.

Evidence of Compartmentalization of *D. papillatum* ALD

Trypanosomatid OMPDC is fused with orotate phosphoribosyltransferase (OPRT) as OMPDC-OPRT and possesses a C-terminal PTS (PTS1), whereas *D. papillatum* OMPDC is a stand-alone enzyme lacking PTSs (Makiuchi et al. 2008). Since PTS2 is present in *D. papillatum* ALD, the ALD and OMPDC may be localized differently in diplonemids. To determine their cellular localizations, we performed western blot analysis of the *D. papillatum* subcellular fractions using specific antibodies to *D. papillatum* ALD and OMPDC (Fig. 1B).

We first confirmed the specificity of the antibody raised against *D. papillatum* ALD by western blotting (Fig. 1B, left). Immunoprecipitates of extracts of both *D. papillatum* and *T. cruzi* using anti-DpALD antibody showed bands at 41 kD, as expected, which were confirmed as aldolase by LC-MS/MS analysis (Supplementary Table S1)

D. papillatum ALD was detected predominantly in the membrane-rich fraction (105,000 ×*g* sediment, lane 3, middle) but not in the cytosolic fraction (105,000 ×*g* supernatant; lane 2, middle). In contrast, OMPDC was detected predominantly in the cytosolic fraction (105,000 ×*g* supernatant; lane 2, right). These results suggest that, in *D. papillatum,* ALD is membrane-associated and likely to be localized in peroxisome-related organelles, whereas OMPDC is a cytosolic protein.

Different Subcellular Distributions of ALD and OPMDC in *D. papillatum*

We further examined the localization of ALD and OMPDC by indirect immunofluorescence analysis. ALD was detected as "*dots*" in both *D. papillatum* and *T. cruzi* (Fig. 3). Confocal fluorescence microscopy showed that the fluorescence signals of mitochondrial DNA and ALD did not merge (Fig. 3, bottom), suggesting that ALD is not a mitochondrial protein and that ALD is compartmentalized into peroxisome-related organelles in both species. In contrast, *D. papillatum* OMPDC was detected throughout the cells and did not co-localize with ALD, again suggesting that OMPDC is a cytosolic protein. Taken together, these findings suggest that, in *D. papillatum,* ALD and OMPDC are separately localized in peroxisome-related compartments and the cytosol, respectively.

Discussion

This is the first report suggesting that, in diplonemids, a glycolytic enzyme is

compartmentalized in peroxisome-related organelles. At present, the biochemical properties of glycolytic enzymes in diplonemids are largely unknown; only partial nucleotide sequences for the fifth enzyme, glyceraldehyde 3-phosphate dehydrogenase (GAPDH), have been cloned but their cellular localization is unknown (Qian and Keeling 2001).

The presence of PTS suggested that peroxisomes are most likely to be the ALD-associated organelles. The presence of ALD in other organelles, such as the mitochondrion and endoplasmic reticulum, is unlikely. The mitochondrion of *D. papillatum* is large and highly branched throughout the cell (Marande et al. 2005). We found, however, that the fluorescence signal of mitochondrial DNA did not co-localize with that of ALD. Moreover, the predicted signal sequences by MitoProt (http://ihg2.helmholtz-muenchen.de/ihg/mitoprot.html) and SignalP (http://www.cbs.dtu.dk/services/SignalP/) indicated that it was unlikely that *D. papillatum* ALD had been imported into the mitochondrion (probability, 0.1330) or endoplasmic reticulum (probability, 0.000).

Glycosomes contain the first seven of the ten enzymes of glycolysis (Michels et al. 2006). In general, the accumulation or compartmentalization of enzymes involved in a metabolic pathway is advantageous for concerted metabolism. This may occur by the formation of enzyme complexes or the fusion of functionally related enzymes. This, however, does not seem true for glycosomes. The compartmentalization of glycolytic enzymes appears physiologically critical for trypanosomatids, especially because hexokinase and 6-phosphofructokinase, the allosteric enzymes that regulate glycolysis in canonical eukaryotes and catalyze the reactions upstream of ALD, are insensitive to their allosteric inhibitors (Michels et al. 2006). The occurrence of these enzymes in the cytosol may result in the accumulation of toxic glycolytic intermediates and the consumption of cytosolic ATP (Bakker et al. 2000). The compartmentalization of glycolytic enzymes may have resulted in the feedback regulation of hexokinase and 6-phosphofructokinase becoming redundant and finally lost, causing their compartmentalization to be critical.

Notably, OMPDC is localized differently in kinetoplastids and diplonemids. Glycosomes also contain enzymes involved in gluconeogenesis, nucleotide biosynthesis, and sugar-nucleotide biosynthesis (Michels et al. 2006). One sugar-nucleotide, UDP-GlcNAc, has been predicted to be an important metabolite in the synthesis of glycosylphosphatidylinositol (GPI)-anchored glycoproteins, which are essential components in trypanosomatids (Ferguson 1999; Stokes et al. 2008). It is important to know whether the enzymes of non-glycolysis pathways became compartmentalized in a common ancestor of diplonemids/kinetoplastids.

We previously showed that, after separation of the kinetoplastid and diplonemid lineages, a common ancestor of kinetoplastids acquired the OMPDC gene by lateral gene transfer, and that this gene subsequently fused with the OPRT gene (Makiuchi et al. 2008). Thus, glycolytic enzymes likely accumulated in the peroxisomes of a common ancestor of kinetoplastids and diplonemids. After the separation of the kinetoplastid lineage, the compartmentalization of other enzymes, including OMPDC (-OPRT fusion), into peroxisome-derived organelles may have occurred, resulting in the formation of glycosomes.

It is worth noting that glycosomes of the parasitic bodonids, *Trypanoplasma borreli* and *Cryptobia salmositica,* possess catalase activity, an authentic peroxisome marker enzyme (Ardelli et al. 2000; Opperdoes et al. 1988). In conjunction with the notion that trypanosomatids are monophyletic and nested within the bodonid clade, stepwise evolution of peroxisome-related organelles in each lineage may have occurred in association with the acquisition and/or loss of the related genes in a lineage-specific manner.

Our findings not only unite kinetoplastids and diplonemids at the level of peroxisome evolution but provide evidence of the diversification of these organelles in Euglenozoa. Further identification of the enzymes involved in the specialized peroxisomes of both lineages would clarify their physiological and biochemical importance.

Methods

Organisms: An axenic culture of *D. papillatum* (ATCC 50162) was routinely maintained as described (Makiuchi et al. 2008). *T. cruzi* Tulahuen strain was maintained in LIT medium (Annoura et al. 2005).

cDNA cloning of the *ALD* gene from *D. papillatum*: The full-length *D. papillatum* ALD cDNA was obtained by 5'- and 3'-RACEs using the partial sequence of a putative *ALD* gene (GenBank™; EC842358, TBestDB;

DPL00001327) registered in the TBest database and the following primer sets: for 5'-RACE, 5'-CGTCGAACTTCTGGGTAAGG-3' (cDNA synthesis), 5'-GCTACAGTTTCTGTACTTTATTG-3' (sense PCR primer, spliced-leader specific), and 5'-ATGACACCGCTGATGTACTG-3' (antisense primer) (Sturm et al. 2001); for 3'-RACE, 5'-AATAAAGCGGCCGCGGATCCAATTTTTTTT TTTTTTTTVN-3' (cDNA synthesis), 5'-GCTGCGACAAGCGCTTCAAG-3' (amplification of the sense strand), 5'-AGACGCTACCGTGCCCTGAT-3' (sense PCR primer), and 5'-AATAAAGCGGCCGCGGATCCAA-3' (antisense primer). Finally, the full-length ALD cDNA was PCR amplified using the primers 5'-CACCATGTCTGCCCGTATCGAAGTCCTGA-3' (sense) and 5'-CTAGTAGGTGTTGCCCTTGATGTAC-3' (antisense) and *D. papillatum* cDNA as a template.

Phylogenetic analysis: All sequence data, with the exception of that of *D. papillatum* ALD cloned by us and first reported here, were collected from public sequence databases by taxonomic and BLAST searches. The sequences reported in this paper appear in the DDBJ/EMBL/GenBank databases under accession number AB550707 for *Diplonema papillatum* ALD mRNA. Multiple alignment of ALD sequences was obtained using CLUSTAL W (Thompson et al. 1994), with the alignment corrected by manual inspection. Unambiguously aligned positions were selected and used for phylogenetic analyses, which were performed by the maximum likelihood (ML), maximum parsimony (MP), and distance matrix (DM) methods implemented in the PHYLIP3.69 package, and by the ML method in the PAML package (Felsenstein ; Yang 1997). With 33 taxa, 310 unambiguously aligned amino acid sites were used for analysis, corresponding to residues 81-105, 107-157, 166-174, 179-225, 240-250, 255-260, 265-281, 290-308 and 317-361 of the *D. papillatum* sequence.

Expression of recombinant *D. papillatum* ALD and OMPDC: The full-length PCR products for the *ALD* and *OMPDC* genes of *D. papillatum* were subcloned in the pET151 expression vector (Invitrogen), which allows N-terminal fusion with His_6-tag, and sequenced. After transformation of *Escherichia coli* BL21-CodonPlus® (DE3)-RP cells (STRATAGENE®, Agilent Technologies, Inc., CA, USA) with the plasmids, expression of ALD and OMPDC was induced by incubation at 25°C in the presence of IPTG. The recombinant proteins were affinity-purified with His•Bind® resin (Novagen, EMD Biosciences, Inc., Madison, WI, USA), equilibrated with phosphate-buffered saline (PBS, pH 7.2), cleaved with AcTEV™ Protease (Invitrogen) to remove the tag and, finally purified further on a His•Bind® column.

Antibodies: Female BALB/c mice were immunized with 100 μg recombinant ALD, and female Japanese white rabbits were immunized with 200 μg OMPDC, each in Freund's complete adjuvant, followed by booster injections with the same antigens in Freund's incomplete adjuvant. IgG was purified from each antiserum using HiTrap™ Protein G HP (GE Healthcare).

Subcellular fractionation, immunoprecipitation, and Western blotting: *D. papillatum* cells were washed once with artificial seawater and twice with 25 mM Tris-HCl/10 mM KCl/1 mM EDTA/250 mM sucrose (pH 7.4). The cells were homogenized in the latter buffer containing a protease inhibitor cocktail (Complete Mini, Roche Diagnostics K.K., Tokyo, Japan) using a cell disruption bomb (Parr Instrument Company, Moline, IL, USA) at 250 psi for 10 min. The homogenates were centrifuged twice at 1,000 ×*g* for 10 min and the supernatant was centrifuged at 105,000 × *g* for 1 hour. The resulting pellet and supernatant were defined as the membrane-rich and cytosolic fractions, respectively. For immunoprecipitation, the cells were harvested by centrifugation at 1,700 ×*g* for 10 min at 4 °C and washed once with PBS (pH 7.2) by centrifugation at 1,700 ×*g* for 10 min at 4 °C. Using an ultrasonicator, the cells were lysed in 10 mM Tris-HCl/150 mM NaCl/1 % TritonX-100/0.5 % NP-40 (pH 8.0) supplemented with the protease inhibitor cocktail. The cell lysates, each containing 140 μg protein, were incubated with the antibody and precipitated using Protein G Magnetic Beads (New England Biolabs, Beverly, MA). The resulting precipitates were separated by SDS-PAGE and transferred to PVDF membranes, which were incubated with the corresponding antibody. Antibody reactions were visualized using alkaline phosphatase-conjugated secondary antibody and a chemiluminescent substrate (CSPD, Roche Diagnostics).

Immunofluorescence microscopy: *D. papillatum* cells were allowed to adhere onto poly-L-lysine coated slides for 15 min in a humidity chamber at 4 °C. After removal of unbound cells, the bound cells were fixed for 25 min with 4% paraformaldehyde and permeabilized in PBS containing 0.5% Triton-X 100 for 10 min at 4 °C. The slides were

incubated in blocking solution (PBS containing 0.05% Tween 20 and 1% BSA) for 30 min, and subsequently with the specific antibody in blocking solution for 90 min at room temperature. After washing with PBS, the slides were incubated with secondary antibodies and counterstained for 10 min with Hoechst 33342 for immunofluorescence microscopy or Hoechst 33258 for confocal laser microscopy. The localization of each enzyme was assessed by fluorescence microscopy.

Acknowledgements

We thank Tsutomu Fujimura, Reiko Mineki, and Hikari Taka of the Division of Proteomics and Biomolecular Science, Biomedical Research Center at Juntendo University Graduate School of Medicine, for mass-spectrometric analysis. This work was supported in part by grants-in-aid for scientific research Nos. 20790327, 18890188 (to T. Annoura) and 19590436 (to T. Nara) and by 21st Century COE Research (to T. Annoura, T. Makiuchi and T. Aoki) from the Ministry of Education, Sports, Culture, Science, and Technology of Japan.

Appendix A. Supplementary materials

Supplementary information is available at Protist online (http://www.elsevier.de/protist).

References

Annoura T, Nara T, Makiuchi T, Hashimoto T, Aoki T (2005) The origin of dihydroorotate dehydrogenase genes of kinetoplastids, with special reference to their biological significance and adaptation to anaerobic, parasitic conditions. J Mol Evol **60**: 113-127

Ardelli BF, Witt JD, Woo PT (2000) Identification of glycosomes and metabolic end products in pathogenic and nonpathogenic strains of *Cryptobia salmositica* (Kinetoplastida: Bodonidae). Dis Aquat Organ **42**: 41-51

Bakker BM, Mensonides FI, Teusink B, van Hoek P, Michels PA, Westerhoff HV (2000) Compartmentation protects trypanosomes from the dangerous design of glycolysis. Proc Natl Acad Sci USA **97**: 2087-2092

Cavalier-Smith T (1981) Eukaryote kingdoms: seven or nine? Biosystems **14**: 461-481

Collins N, Merrett MJ (1975) The localization of glycollate-pathway enzymes in *Euglena*. Biochem J **148**: 321-328

Felsenstein J. *PHYLIP*. Available from: http://evolution.gs.washington.edu/phylip.html.

Ferguson MA (1999) The structure, biosynthesis and functions of glycosylphosphatidylinositol anchors, and the contributions of trypanosome research. J Cell Sci **112 (Pt 17)**: 2799-2809

Gabaldón T (2010) Peroxisome diversity and evolution. Philos Trans R Soc Lond B Biol Sci **365**: 765-773

Gabaldón T, Snel B, van Zimmeren F, Hemrika W, Tabak H, Huynen MA (2006) Origin and evolution of the peroxisomal proteome. Biol Direct **1**: 8

Graves LB, Jr., Hanzely L, Trelease RN (1971) The occurrence and fine structural characterization of microbodies in *Euglena gracilis*. Protoplasma **72**: 141-152

Hammond DJ, Gutteridge WE (1982) UMP synthesis in the kinetoplastida. Biochim Biophys Acta **718**: 1-10

Hart DT, Misset O, Edwards SW, Opperdoes FR (1984) A comparison of the glycosomes (microbodies) isolated from *Trypanosoma brucei* bloodstream form and cultured procyclic trypomastigotes. Mol Biochem Parasitol **12**: 25-35

Hayashi M, Toriyama K, Kondo M, Kato A, Mano S, De Bellis L, Hayashi-Ishimaru Y, Yamaguchi K, Hayashi H, Nishimura M (2000) Functional transformation of plant peroxisomes. Cell Biochem Biophys **32**: 295-304

Makiuchi T, Nara T, Annoura T, Hashimoto T, Aoki T (2007) Occurrence of multiple, independent gene fusion events for the fifth and sixth enzymes of pyrimidine biosynthesis in different eukaryotic groups. Gene **394**: 78-86

Makiuchi T, Annoura T, Hashimoto T, Murata E, Aoki T, Nara T (2008) Evolutionary analysis of synteny and gene fusion for pyrimidine biosynthetic enzymes in Euglenozoa: an extraordinary gap between kinetoplastids and diplonemids. Protist **159**: 459-470

Marande W, Lukeš J, Burger G (2005) Unique mitochondrial genome structure in diplonemids, the sister group of kinetoplastids. Eukaryot Cell **4**: 1137-1146

Michels PA, Hannaert V, Bringaud F (2000) Metabolic aspects of glycosomes in trypanosomatidae - new data and views. Parasitol Today **16**: 482-489

Michels PA, Bringaud F, Herman M, Hannaert V (2006) Metabolic functions of glycosomes in trypanosomatids. Biochim Biophys Acta **1763**: 1463-1477

Michels PA, Moyersoen J, Krazy H, Galland N, Herman M, Hannaert V (2005) Peroxisomes, glyoxysomes and glycosomes (review). Mol Membr Biol **22**: 133-145

Opperdoes FR, Borst P (1977) Localization of nine glycolytic enzymes in a microbody-like organelle in *Trypanosoma brucei*: the glycosome. FEBS Lett **80**: 360-364

Opperdoes FR, Nohynkova E, Van Schaftingen E, Lambeir AM, Veenhuis M, Van Roy J (1988) Demonstration of glycosomes (microbodies) in the Bodonid flagellate *Trypanoplasma borelli* (Protozoa, Kinetoplastida). Mol Biochem Parasitol **30**: 155-163

Parsons M, Furuya T, Pal S, Kessler P (2001) Biogenesis and function of peroxisomes and glycosomes. Mol Biochem Parasitol **115**: 19-28

Plaumann M, Pelzer-Reith B, Martin WF, Schnarrenberger C (1997) Multiple recruitment of class-I aldolase to chloroplasts and eubacterial origin of eukaryotic class-II aldolases revealed by cDNAs from *Euglena gracilis*. Curr Genet **31**: 430-438

Qian Q, Keeling PJ (2001) Diplonemid glyceraldehyde-3-phosphate dehydrogenase (GAPDH) and prokaryote-to-eukaryote lateral gene transfer. Protist **152**: 193-201

Rutter WJ (1964) Evolution of Aldolase. Fed Proc **23**: 1248-1257

Schlüter A, Fourcade S, Ripp R, Mandel JL, Poch O, Pujol A (2006) The evolutionary origin of peroxisomes: an ER-peroxisome connection. Mol Biol Evol **23**: 838-845

Shigeoka S, Nakano Y, Kitaoka S (1980) Metabolism of hydrogen peroxide in *Euglena gracilis* Z by L-ascorbic acid peroxidase. Biochem J **186**: 377-380

Simpson AG, Roger AJ (2004) Protein phylogenies robustly resolve the deep-level relationships within Euglenozoa. Mol Phylogenet Evol **30**: 201-212

Simpson AG, Lukeš J, Roger AJ (2002) The evolutionary history of kinetoplastids and their kinetoplasts. Mol Biol Evol **19**: 2071-2083

St-Jean M, Lafrance-Vanasse J, Liotard B, Sygusch J (2005) High resolution reaction intermediates of rabbit muscle fructose-1,6-bisphosphate aldolase: substrate cleavage and induced fit. J Biol Chem **280**: 27262-27270

Stokes MJ, Guther ML, Turnock DC, Prescott AR, Martin KL, Alphey MS, Ferguson MA (2008) The synthesis of UDP-N-acetylglucosamine is essential for bloodstream form *Trypanosoma brucei* in vitro and in vivo and UDP-N-acetylglucosamine starvation reveals a hierarchy in parasite protein glycosylation. J Biol Chem **283**: 16147-16161

Sturm NR, Maslov DA, Grisard EC, Campbell DA (2001) *Diplonema* spp. possess spliced leader RNA genes similar to the Kinetoplastida. J Eukaryot Microbiol **48**: 325-331

Taylor MB, Gutteridge WE (1987) *Trypanosoma cruzi*: subcellular distribution of glycolytic and some related enzymes of epimastigotes. Exp Parasitol **63**: 84-97

Thompson JD, Higgins DG, Gibson TJ (1994) CLUSTAL W: improving the sensitivity of progressive multiple sequence alignment through sequence weighting, position-specific gap penalties and weight matrix choice. Nucleic Acids Res **22**: 4673-4680

Tolbert NE, Oeser A, Kisaki T, Hageman RH, Yamazaki RK (1968) Peroxisomes from spinach leaves containing enzymes related to glycolate metabolism. J Biol Chem **243**: 5179-5184

Walther R, Wasternack C, Helbing D, Lippmann G (1980) Pyrimidine metabolizing enzymes in *Euglena gracilis*: Synthesis and localization of OPRTase, ODCase and β -ureidopropionase. Biochem Physiol Pflanzen **175**: 764-771

Yang Z (1997) PAML: a program package for phylogenetic analysis by maximum likelihood. Comput Appl Biosci **13**: 555-556

Figure Legends

Figure 1. Characterization of aldolase (ALD) of *Diplonema papillatum*. (**A**) Amino acid sequence alignment of Class I fructose-1,6-bisphosphate aldolases. The asterisks indicate the same or equivalent amino acids. The N-terminal peroxisomal targeting signals (PTS2), consisting of a consensus nonapeptide (R/K)-(L/V/I)-X_5-(Q/H)-(L/A), are shaded. (**B**) Western blot analysis of ALD (41 kD) (left and middle panels) and orotidine-5'-monophosphate decarboxylase (OMPDC, 25 kD) (right panel) of *D. papillatum*. The anti-ALD antibody specifically recognizes ALD of *Trypanosoma cruzi* (Tc) and *D. papillatum* (Dp) (left panel). The crude cell lysate (lane 1), supernatant (lane 2) and precipitate (lane 3) of a 105,000 × *g* preparation were reacted with the specific antibodies. The arrow and arrowheads indicate the bands for ALD (41 kD) and the precipitated antibodies, respectively.

Figure 2. Phylogenetic reconstruction of Class I fructose-1,6-bisphosphatae aldolase (ALD). The consensus maximum likelihood (ML) tree of ALD inferred by the JTT model taking across-site rate heterogeneity into consideration. The α-value of the Γ shape parameter used in the analysis was 0.85937. Bootstrap proportions (BPs) by the ML method are attached to the internal branches. Branches with less than 50% BP support are unmarked. For the four nodes, BP values determined by the distance matrix (DM) and maximum parsimony (MP) methods are also shown.

Figure 3. Indirect immunofluorescence analyses of *T. cruzi* and *D. papillatum*. *T. cruzi* (Tc, top) and *D. papillatum* (Dp, middle) were fixed, reacted with anti-*D. papillatum* ALD antibody, conjugated with Alexa Fluor 488, and counterstained with Hoechst 33342. Localization of ALD and OMPDC in *D. papillatum* cells was assessed by confocal microscopy (bottom, counterstained with Hoechst 33258). Neither pre-immune sera nor the antiserum absorbed with the corresponding antigens showed any fluorescent signal. DIC, differential interference contrast image; Merged, merged image. Scale bar = 5 μm.

Makiuchi *et al.* Figure 1.

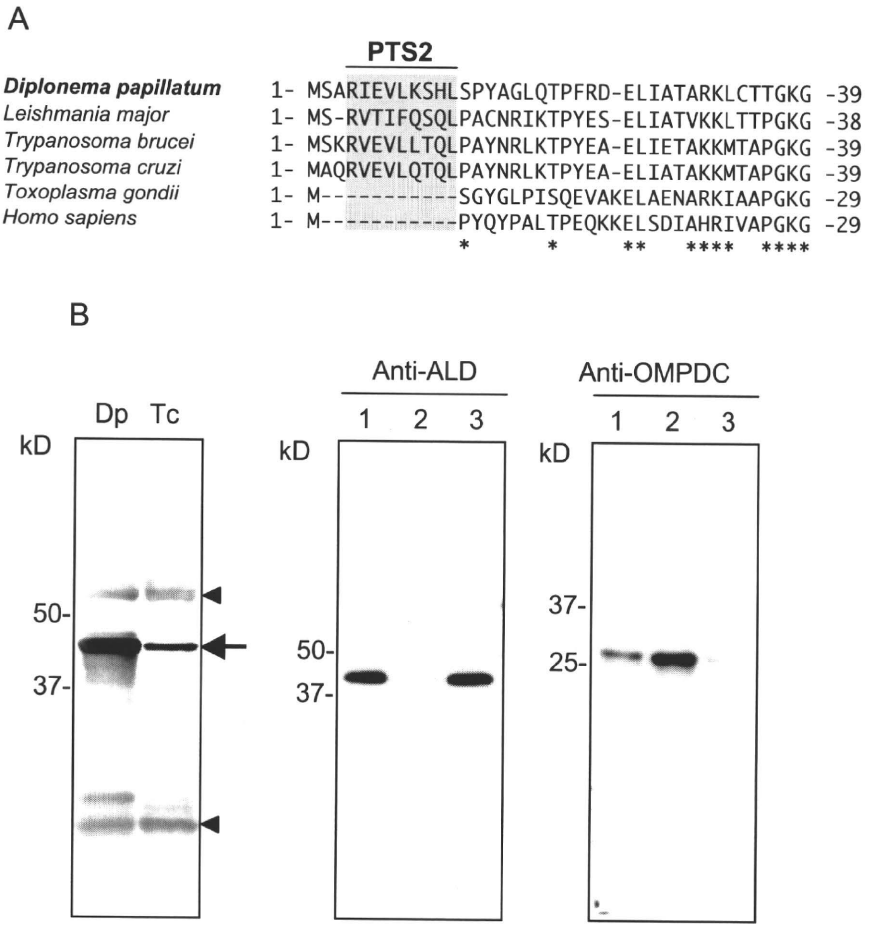

Makiuchi *et al.* Figure 2.

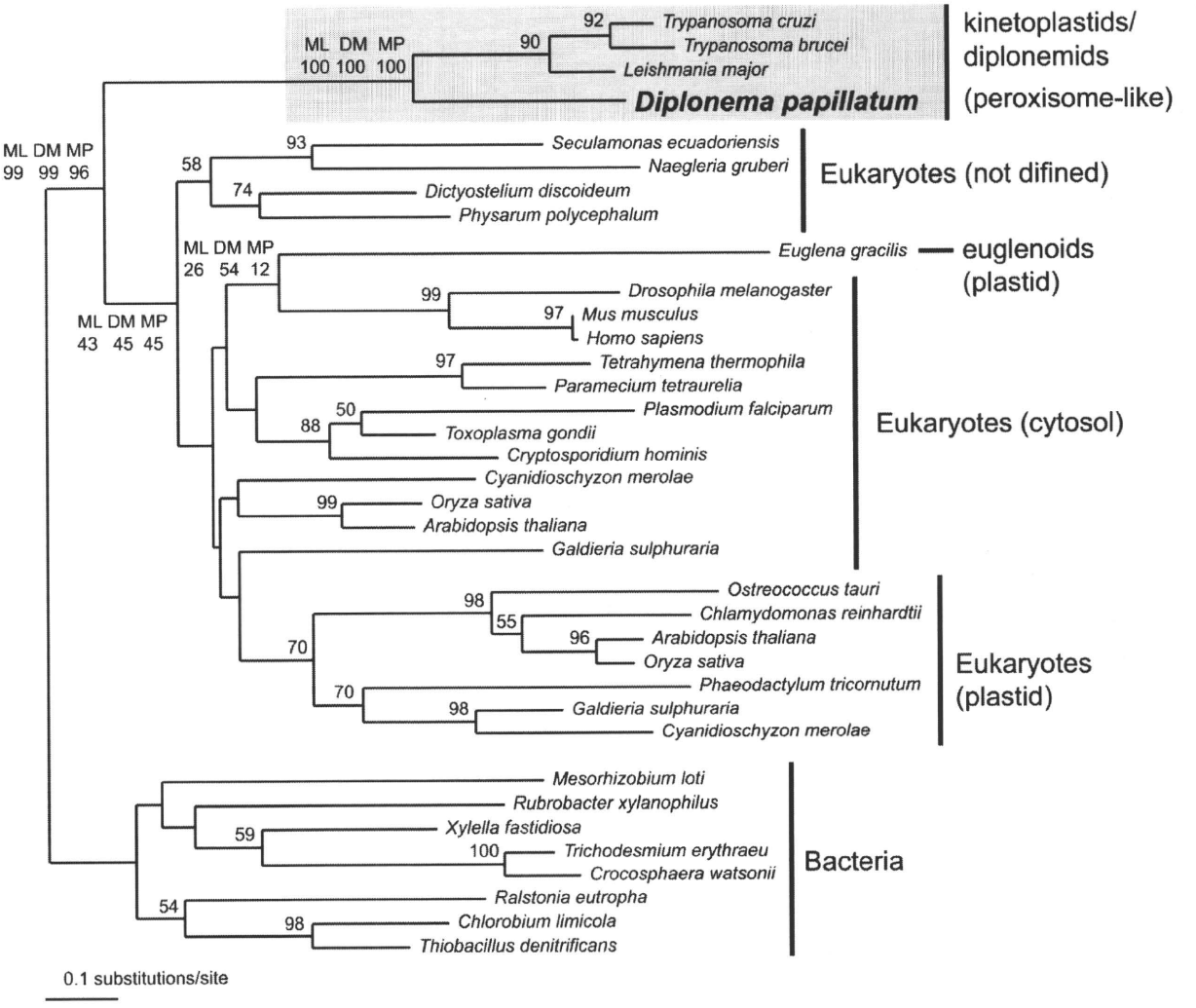

Makiuchi *et al.* Figure 3.

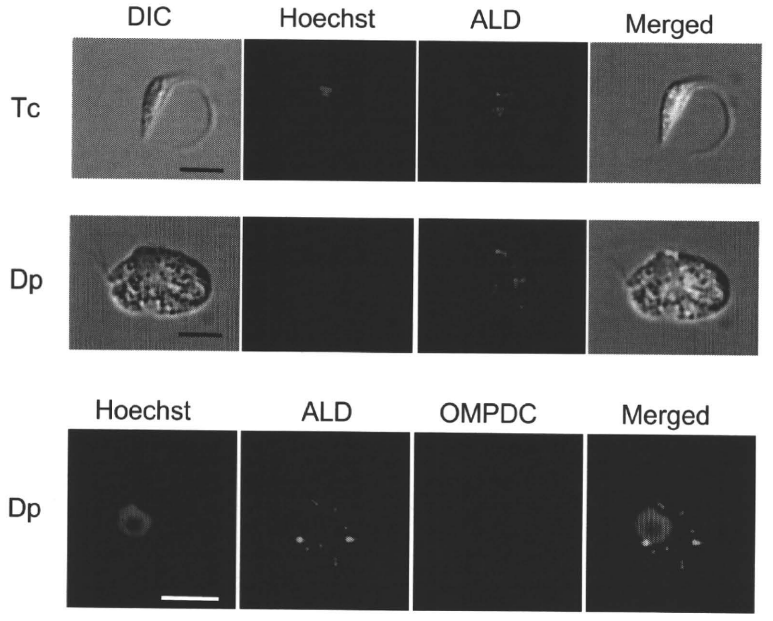

Supplementary Materials and Methods

In-gel digestion and liquid chromatography-tandem mass spectrometry (LC-MS/MS)

In-gel trypsin digestion of SDS–PAGE bands of interest was performed as described (Mineki et al. 2002). The protein(s) in each band were digested with trypsin, eluted from the gel, and dissolved in 10 μl 1% formic acid. Mass spectrometry was performed using an AB-QSTAR pulsar *i* hybrid (Applied Biosystems, Inc., Framingham, CA) and a micro-liquid chromatograph (Magic 2002; Michrom Bioresources, Inc., Abum, CA) equipped with a 0.2-mm ID × 50 mm Magic C18 column. The amino acid sequences of the peptides were assessed by LC-MS/MS, with a Mascot search engine (www.matrixscience.com/search_form_select.html) used for all peptide mass mapping and MS/MS ion searching against the proteome database, NCBInr.

References

Mineki R, Taka H, Fujimura T, Kikkawa M, Shindo N, Murayama K (2002) In situ alkylation with acrylamide for identification of cysteinyl residues in proteins during one- and two-dimensional sodium dodecyl sulphate-polyacrylamide gel electrophoresis. Proteomics **2**: 1672-1681

Supplementary Table S1. Amino acid sequences of polypeptides, identified by liquid chromatography-tandem mass spectrometry, specific for *D. papillatum* and *T. cruzi* native ALDs.

Species	Sequence	*Mr* (expt)	*Mr* (calc)
D. papillatum	^{32}KLCTTGK^{38}	820.42	820.45
	^{39}GLLAADESQGSCDK^{52}	1463.61	1463.66
	^{39}GLLAADESQGSCDKR^{53}	1619.68	1619.76
	^{54}FKPIGLPNNEENR^{66}	1526.75	1526.78
	^{102}SFPELCNSLGIVPGIK^{117}	1743.83	1743.92
	^{118}TDKGLVDAVGGAPGEQATQGLDNYEK^{143}	2632.17	2632.26
	^{121}GLVDAVGGAPGEQATQGLDNYEK^{143}	2288.01	2288.09
	^{121}GLVDAVGGAPGEQATQGLDNYEKR^{144}	2444.11	2444.19
	^{184}YAQLSQK^{190}	836.40	836.44
	^{191}QGLVPIVEPEVMIDGNHDIAACQAVSQR^{218}	3042.58	3042.49
	^{219}VWAEVVR^{225}	857.45	857.48
	^{262}ATLTTLAR^{269}	845.46	845.50
	^{316}ALQASALK^{323}	800.43	800.48
	^{324}AWGGKEENK^{332}	1017.44	1017.49
	^{345}MNSLATLGK^{353}	933.47	933.50
	^{354}YNPGEDSK^{361}	908.34	908.39
	^{365}ESLYIK^{370}	751.38	751.41
T. cruzi	^{20}TPHEAELIATAK^{31}	1279.68	1279.68
	^{32}KMTAPGK^{38}	747.39	747.39
	^{33}MTAPGK^{38}	603.30	603.31
	^{54}FAPLGLSNTEEHR^{66}	1469.71	1469.73
	^{97}ASTGETFVQLLQR^{109}	1448.78	1448.76
	^{110}KGVVPGIK^{117}	796.52	796.52
	^{111}GVVPGIK^{117}	668.43	668.42
	^{118}TDMGLNPLVEGAEGEQMTGGLDGYVER^{144}	2853.28	2853.28
	^{148}YYSLGCR^{154}	931.43	931.42
	^{160}NVYK^{163}	522.28	522.28
	^{164}IQNGTVSEAAVR^{175}	1243.66	1243.65
	^{176}FNAETLAR^{183}	920.47	920.47
	^{254}ATPGQVAQYTVSTLAR^{269}	1661.89	1661.87
	^{308}LTFSYAR^{314}	856.44	856.44
	^{315}ALQSSALK^{322}	816.47	816.47
	^{328}DSGIAAGR^{335}	745.37	745.37
	^{337}AFMHRAK^{341}	660.32	660.32
	^{342}AKMNSLAQLGR^{352}	1203.67	1203.64
	^{344}MNSLAQLGR^{352}	988.50	988.51
	^{356}AEDDKESHSLYVAGNSY^{372}	1883.82	1883.82

Mr (expt) and *Mr* (calc) denote the experimentally determined and calculated molecular masses, respectively. Delta values (experimental minus calculated) of less than ±0.1 are considered highly specific.

Oncogene (2010), 1–11

www.nature.com/onc

ORIGINAL ARTICLE

Osteopontin-mediated enhanced hyaluronan binding induces multidrug resistance in mesothelioma cells

K Tajima[1,2], R Ohashi[1,2], Y Sekido[3], T Hida[3], T Nara[4], M Hashimoto[4], S Iwakami[5], K Minakata[1,2], T Yae[1,6], F Takahashi[1,2], H Saya[6] and K Takahashi[1,2]

[1]Department of Respiratory Medicine, Juntendo University, School of Medicine, Bunkyo-Ku, Tokyo, Japan; [2]Research Institute for Diseases of Old Ages, Juntendo University, School of Medicine, Bunkyo-Ku, Tokyo, Japan; [3]Division of Molecular Oncology, Aichi Cancer Center Research Institute, Chikusa-ku, Nagoya, Japan; [4]Department of Molecular and Cellular Parasitology, Juntendo University, School of Medicine, Bunkyo-Ku, Tokyo, Japan; [5]Department of Respiratory Medicine, Juntendo University Shizuoka Hospital, Shizuoka, Japan and [6]Division of Gene Regulation Institute for Advanced Medical Research School of Medicine, Keio University, Shinjuku-Ku, Tokyo, Japan

Malignant pleural mesothelioma (MPM) is resistant to chemotherapy and thus shows a dismal prognosis. Osteopontin (OPN), a secreted noncollagenous and phosphoprotein, is suggested to be involved in the pathogenesis of MPM. However, the precise role of OPN, especially in the multidrug resistance of MPM, remains to be elucidated. We therefore established stable transfectants (ACC-MESO-1/OPN), which constitutively express OPN, to determine its role in the chemoresistance observed in MPM. The introduction of the OPN gene provides MPM cells with upregulated multidrug resistance through the mechanism of enhanced hyaluronate (HA) binding. The expression of CD44 variant isoforms, which inhibit HA binding, significantly decreased in ACC–MESO–1/OPN cells in comparison to control transfectants. Interestingly, the inhibition of the HA-CD44 interaction abrogated multidrug resistance in the ACC–MESO–1/OPN, thus suggesting the involvement of the surviving signal emanating from the HA-CD44 interaction. An enhanced level of the p-Akt in ACC–MESO–1/OPN cells was observed, and was diminished by CD44 siRNA. Inhibition of the Akt phosphorylation increased in number of the cells underwent apoptosis induced by NVB, VP-16 and GEM. Collectively, these results indicate that OPN is strongly involved in multidrug resistance by enhancing the CD44 binding to HA.
Oncogene advance online publication, 18 January 2010; doi:10.1038/onc.2009.478

Keywords: osteopontin; mesothelioma; multidrug resistance; hyaluronan; CD44

Introduction

Malignant pleural mesothelioma (MPM) is an extremely aggressive tumor, which has been shown to be resistant to all conventional therapeutic regimens. A surgical resection is possible in only a minority of patients, and fewer than 15% of these patients live beyond 5 years (Sugarbaker *et al.*, 1996; Boutin *et al.*, 1998; Rusch and Venkatraman, 1999). For those who are not treated with a curative resection, the median survival has been reported to be 6 months (Ruffie, 1991; De Pangher Manzini *et al.*, 1993). As a result, chemotherapy is still the mainstay of disease therapy. Various drugs including doxorubicin, cyclophosphamide, cisplatin (CDDP), carboplatin, gemcitabine (GEM), and pemetrexed have been tested in different combinations (Samson *et al.*, 1987; Chahinian *et al.*, 1993; White *et al.*, 2000; Kindler *et al.*, 2001; Hughes *et al.*, 2002). However, the limited combinations of these agents have marginally provided some clinical benefit because of multidrug resistance. Moreover, none of the molecular targeting agents have shown any of their clinical benefit in the patients with MPM (Moore *et al.*, 2007; Jackman *et al.*, 2008). Therefore, it is hoped that a better understanding of the mechanism of the multidrug resistance in MPM may provide the rationale for the development of new therapeutic strategies.

Drug resistance arises in numerous ways, such as through a decreased access to or uptake of drugs, the activation of repair and detoxification mechanisms, and an increased drug efflux. Among these numerous mechanisms, resistance against anti-cancer agents has been recently reported upon cell adhesion to the extracellular matrix (ECM) (Damiano *et al.*, 1999; Elliott and Sethi, 2002; Hazlehurst *et al.*, 2003), thus suggesting that tumor–microenvironment interaction regulates the sensitivity of anti-cancer agents. For instance, it has been reported that small cell lung cancer cells, myeloma cells, glioma cells and colon cancer cells were protected from apoptosis induced by various anticancer agents when the cells were plated on ECM (Damiano *et al.*, 1999; Sethi *et al.*, 1999; Uhm *et al.*, 1999; Kouniavsky *et al.*, 2002). MPM cells are surrounded by pleural effusion, which contains a variety of ECM including hyaluronate (HA) and osteopontin (OPN) (Thylen *et al.*, 1997; Pass *et al.*, 2005; Grigoriu *et al.*, 2007). The ability to grow in pleural fluid suggests

Correspondence: Dr K Tajima, Department of Respiratory Medicine, Juntendo University, School of Medicine, 2-1-1 Hongo, Bunkyo-Ku, Tokyo 113-8421, Japan.
E-mail: tajiken@juntendo.ac.jp
Received 31 March 2009; revised 25 October 2009; accepted 2 November 2009

that the MPM cells are capable of surviving and proliferating against apoptosis under the influence of this particular microenvironment. These findings indicate that the biological function of MPM appears to be strictly regulated by the interaction with ECM.

OPN, a secreted noncollagenous, phosphoprotein, functions as both an ECM component and cytokine through the binding to its receptors; integrin and CD44 (Denhardt *et al.*, 2001). OPN has been associated with cancer progression, metastasis and apoptosis (Rangaswami *et al.*, 2006). Several studies have revealed elevated levels of OPN in serum and pleural effusion to be observed in patients with MPM (Pass *et al.*, 2005; Grigoriu *et al.*, 2007), thus suggesting the involvement of OPN in the pathogenesis of MPM. In fact, OPN was recently demonstrated to mediate MPM cell proliferation and migration (Ohashi *et al.*, 2009). OPN has also been reported to be involved in resistance to chemotherapy of mouse breast cancer cells by inhibiting apoptosis (Graessmann *et al.*, 2007). However, the role of OPN especially in multidrug resistance in MPM has not yet been clarified.

HA is a linear glycosaminoglycan, which is ubiquitously distributed in the ECM, and interacts with cell surface receptors including CD44 (Toole, 2004). HA facilitates cell adhesion, cell motility, cellular proliferation and tumor progression (Lokeshwar *et al.*, 1997). An increased HA production was found to upregulate drug resistance in cancer cells (Misra *et al.*, 2003). It is therefore possible that the effect of CD44 binding to HA on cell-survival signaling might alter drug resistance. In fact, HA–CD44 interaction was recently revealed to have a pivotal role in the chemoresistance in non-small cell lung cancer cells (Ohashi *et al.*, 2007). Very interestingly, recent studies have strongly supported the notion that the OPN could modulate the CD44 isoform expression, which closely regulates HA binding. For instance, Khan *et al.* (2005) reported that OPN modulates the specific CD44 isoform expression to facilitate breast cancer cell migration. Moreover, an overexpression of endogenous OPN results in increased hyaruronan synthase 2 activities, thus leading to an increased HA production and an enhanced anchorage-independent growth (Cook *et al.*, 2006).

Based on these findings, we hypothesized that OPN could regulate chemosensitivity through the alteration of CD44 binding to HA. We also discuss the potential mechanisms of the multidrug resistance in MPM.

Results

Generation of stable transfectant that secretes OPN

BMGNeo–OPN and BMGNeo were transfected into the ACC-MESO-1 cells and we thus obtained two stable OPN-overexpressing clones (ACC-MESO-1/OPN#7 and ACC-MESO-1/OPN#8) and two control clones (ACC-MESO-1/Neo#1 and ACC-MESO-1/Neo#2). To verify the secretion of OPN protein from the transfectant, we conducted the ELISA for OPN. As shown in Figure 1a, ELISA demonstrated the ACC-MESO-1/OPN cells to secrete significant amounts of OPN.

Transfection with OPN gene result in increased multidrug resistance

The IC_{50} of NVB against OPN7 cells and OPN8 cells were 3.87 ± 0.47 ng/ml and 4.56 ± 0.89 ng/ml, respectively, whereas those against Neo1 cells, Neo2 cells and parental cells were 1.70 ± 0.04 ng/ml, 1.97 ± 0.71 ng/ml and 1.91 ± 0.11 ng/ml, respectively (Figure 1b). The IC_{50} of VP16 against OPN7 cells and OPN8 cells were 8.71 ± 0.34 μM and 15.76 ± 1.49 μM, respectively, whereas those against Neo1 cells, Neo2 cells and parental cells were 4.47 ± 1.51 μM, 3.69 ± 1.00 μM and 2.17 ± 0.19 μM, respectively (Figure 1c). As IC_{50} never reached at any concentration of GEM in OPN transfectants, we could not show the IC_{50} regarding OPN transfectants. The IC_{50} of GEM against Neo1 cells, Neo2 cells and parental cells were 0.05 ± 0.002 μM, 0.03 ± 0.02 μM and 0.04 ± 0.018 μM, respectively (Figure 1d). The IC_{50} of CDDP against OPN7 cells and OPN8 cells were 6.44 ± 0.18 μg/ml and 5.85 ± 0.40 μg/ml, respectively, whereas those against Neo1 cells, Neo2 cells and parental cells were 12.00 ± 1.52 μg/ml, 11.56 ± 2.68 μg/ml and 3.39 ± 1.68 μg/ml, respectively (Figure 1e). These results indicate that the ACC-MESO-1/OPN cells were more resistant to NVB, VP-16 and GEM than the ACC-MESO-1/Neo or parental cells, whereas ACC-MESO-1/OPN cells did not demonstrate resistance to CDDP. We next evaluated the amount of apoptotic cells (Figure 1f). We observed that ACC-MESO-1/OPN cells were more significantly resistant to apoptosis mediated by anticancer agents than ACC-MESO-1/Neo cells. These data indicate that the transfection with OPN gene thus resulted in an increased multidrug resistance. Moreover, transfection with OPN gene also increased resistance to apoptosis induced by NVB, VP-16 and GEM.

OPN regulates cell adhesion to HA

To evaluate the effect of OPN transfected to ACC-MESO-1 cells on OPN or HA binding, an *in vitro* cell adhesion assay was performed using ACC-MESO-1/OPN, ACC-MESO-1/Neo and parental cells. The cells were investigated for adhesion to OPN, HA or BSA (Figure 2a). Interestingly, the ratio of adherence to HA (percent-specific adhesion to HA/percent-specific adhesion to BSA) of ACC-MESO-1/OPN cells was significantly greater than that of the ACC-MESO-1/Neo and parental cells, whereas neither ACC-MESO-1/OPN cells nor ACC-MESO-1/Neo cells demonstrated adherence to OPN (Table 1). To investigate whether the silencing of the OPN expression abrogates enhanced adhesion to HA, we downregulated the OPN expression in ACC-MESO-1/OPN#8 cells by siRNA. siRNA transfection downregulated the OPN expression by >80% (Figure 2b) and then we next performed an adhesion assay. As expected, the silencing of OPN expression in ACC-MESO-1/OPN#8 cells decreased the adhesion to HA (Figure 2c). These results therefore suggest that OPN regulates the cell adhesion to HA.

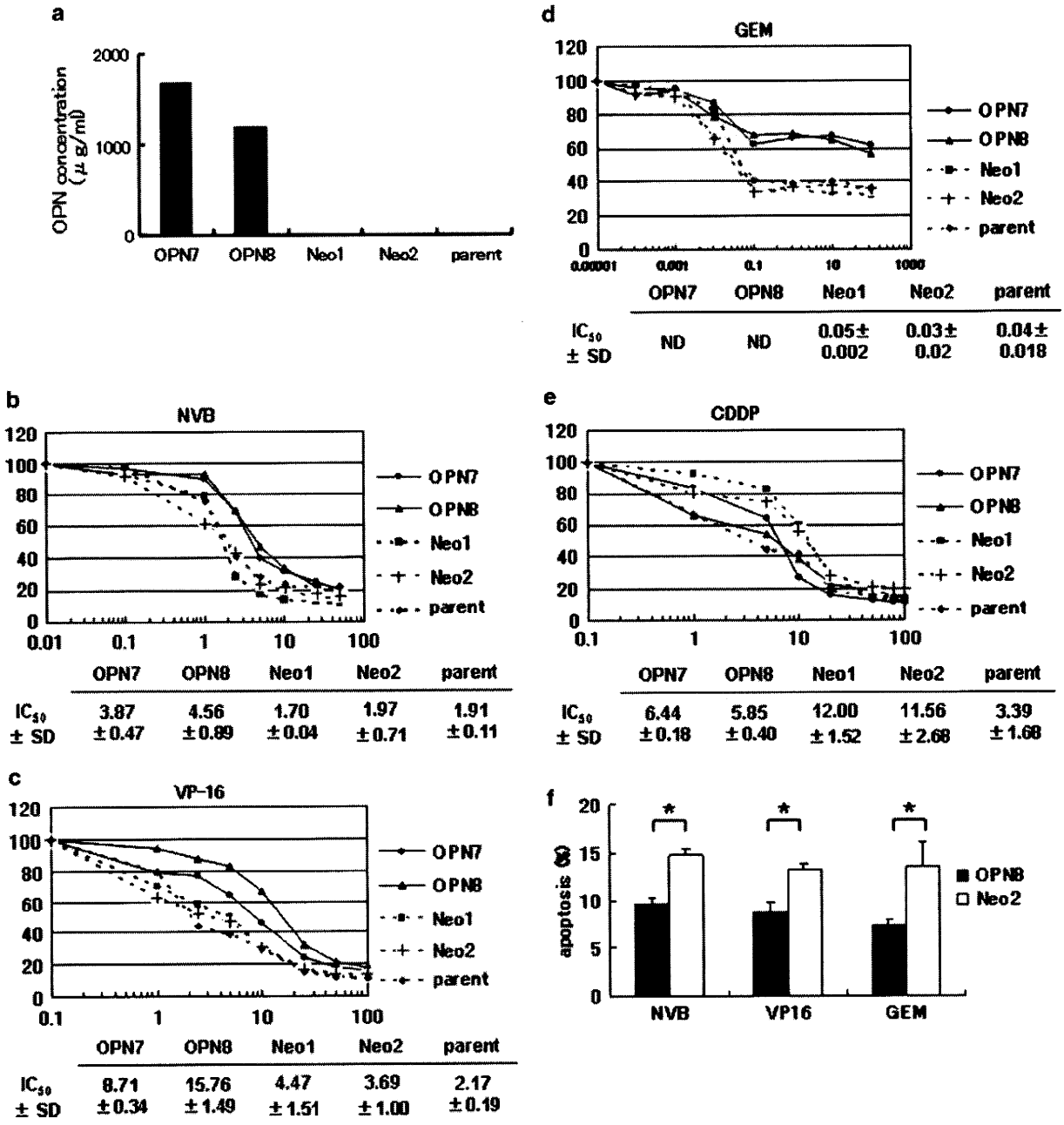

Figure 1 Establishment of ACC-MESO-1 cells transfected with an empty vector (ACC-MESO-1/Neo) or OPN gene (ACC-MESO-1/OPN). (**a**) OPN protein secretion was determined with ELISA. *In vitro* chemosensitivity assay. Both ACC-MESO-1/OPN and ACC-MESO-1/Neo clones were cultured in the absence or the presence of various concentration of vinorelbin (VNB; **b**), etoposide (VP-16; **c**), gemcitabine (GEM; **d**), and cisplatin (CDDP; **e**). Data are representative of the findings of one of three independent experiments with similar results. IC_{50}s are presented as the mean ± s.d. in triplicates. ND: not determined. (**f**) Apoptosis induction was evaluated by Annexin V staining method. ACC-MESO-1/OPN#8 cells were cultured in the presence of VNB (2.5 ng/ml), VP-16 (10 μM) and GEM (0.1 μM). Closed and open squares indicate ACC-MESO-1/OPN#8 and ACC-MESO-1/Neo#2, respectively. Data are presented as the mean ± s.d. of apoptotic cells of three independent experiments. $^*P < 0.05$ vs OPN8.

Expression of CD44 and CD44 variant isoforms

As ACC-MESO-1/OPN cells showed an enhanced adhesion to HA, we therefore compared the expression levels of CD44, a principle receptor for HA, on the surface of ACC-MESO-1/OPN, ACC-MESO-1/Neo and parental cells with FACScan. As shown in Figure 3a, there was no difference in the total CD44 surface expression among ACC-MESO-1/OPN, ACC-MESO-1/Neo and parental cells. As certain CD44 variant isoforms have been reported to display significantly less HA binding than CD44s (Iida and Bourguignon, 1997), we next examined the expression pattern

of the CD44 variant isoforms using RT–PCR (Figure 3b) and western blotting (Figure 3c). It was noteworthy that the fragment of CD44s, which was expected to exhibit a PCR amplification product of 375 bp and several other larger fragments were expressed in each clone, thus suggesting the presence of alternatively spliced transcripts (Figure 3b). To identify these larger fragments, a direct DNA sequence analysis was performed. The 550 bp product corresponds to exon14 (v10), whereas the 750 bp product corresponds to exons12, 13 and 14 (v8, v9 and v10, respectively) (data not shown). CD44 protein expression was analyzed by western blotting using BU52. The expression of high molecular weight CD44 variant isoforms was significantly decreased in the ACC-MESO-1/OPN cells in comparison compared to that of the ACC-MESO-1/Neo and parental cells (Figure 3c). To determine whether exogenous OPN regulates the expression of CD44 variant isoforms on ACC-MESO-1 cells, a western blot analysis was performed to evaluate the CD44 isoform expression on the ACC-MESO-1 cells cultured on OPN and BSA. The expression of high molecular weight CD44 variant isoforms significantly decreased in the ACC-MESO-1 cells cultured on OPN compared with that of the ACC-MESO-1 cells cultured on BSA (Figure 3d).

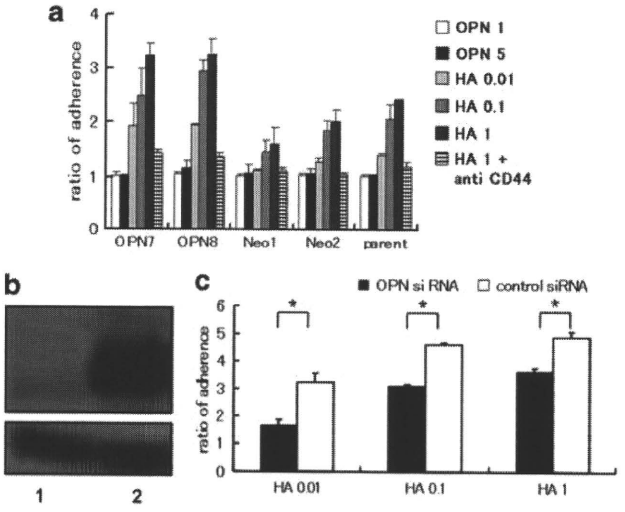

Figure 2 Adhesion assay. *In vitro cell* adhesion assay of ACC-MESO-1/OPN cells and ACC-MESO-1/Neo cells. (**a**) ACC-MESO-1/OPN, ACC-MESO-1/Neo or parental cells, were allowed to adhere to wells coated with OPN (1, 5 μg/ml), HA (0.01, 0.1, 1 mg/ml) or BSA (10 mg/ml) in the presence or absence of anti-CD44 antibody (BU75, 1 μg/ml). Data are presented as the mean ± s.d. in triplicates. (**b**) OPN expression by ACC-MESO-1/OPN cells transfected with OPN siRNA (lane 1) or negative control siRNA (lane 2). OPN protein expression was detected by western blotting. Bottom panel shows β-actin expression as loading control. (**c**) *In vitro* cell adhesion assay was performed using ACC-MESO-1/OPN OPN#8 siRNA and ACC-MESO-1/OPN#8 control siRNA. Closed and open squares indicate OPN siRNA and control siRNA, respectively. Data are presented as the mean ± s.d. in triplicates. $^{*}P<0.05$ vs control siRNA.

Downregulation of CD44v10 expression increases the multidrug resistance

To investigate whether the downregulation of the CD44v10 expression is involved in the mechanism of the multidrug resistance, we downregulated the CD44v10 expression in ACC-MESO-1 cells by siRNA. siRNA transfection downregulated the CD44v10 expression by >80% and then a chemosensitivity assay was performed (Figure 4a). The IC_{50} of NVB against the ACC-MESO-1 cells transfected with CD44v10 siRNA was 17.47 ± 7.00 ng/ml, whereas those against the cells transfected with control siRNA was 2.54 ± 0.31 ng/ml (Figure 4b). The IC_{50} of NVB against the ACC-MESO-1 cells transfected with CD44v10 siRNA was significantly higher than that against the cells transfected with control siRNA ($P<0.05$). The IC_{50} of VP16 against the ACC-MESO-1 cells transfected with CD44v10 siRNA was 10.53 ± 0.11 μM, whereas those against the cells transfected with control siRNA was 2.36 ± 0.20 μM (Figure 4c). The IC_{50} of VP-16 against the ACC-MESO-1 cells transfected with CD44v10 siRNA was significantly higher than that against the cells transfected with control siRNA ($P<0.05$). As IC_{50} was never

Table 1 The ratio of adherence to HA and OPN (percent-specific adhesion to HA or OPN/percent-specific adhesion to BSA)[a]

	OPN 1	*OPN 5*	*HA 0.01*	*HA 0.1*	*HA 1*
OPN7	1.02 ± 0.09	1.00 ± 0.02	1.92 ± 0.40*	2.47 ± 0.48^{+}	3.21 ± 0.24$^{\#,\#\#,\#\#\#}$
OPN8	1.05 ± 0.03	1.15 ± 0.15	1.93 ± 0.01*,**,***	2.93 ± 0.22$^{+,++,+++}$	3.25 ± 0.30$^{\#,\#\#,\#\#\#}$
Neo1	1.02 ± 0.03	1.08 ± 0.15	1.11 ± 0.01	1.45 ± 0.22	1.60 ± 0.30
Neo2	1.03 ± 0.05	1.08 ± 0.09	1.29 ± 0.06	1.85 ± 0.18	2.00 ± 0.21
Parent	1.01 ± 0.05	1.03 ± 0.03	1.40 ± 0.02	2.07 ± 0.24	2.39 ± 0.01

[a]Data are presented as the mean ± s.d. in triplicates.
$^{*}P<0.05$ vs Neo1 cells treated with HA 0.01.
$^{**}P<0.05$ vs Neo2 cells treated with HA 0.01.
$^{***}P<0.05$ vs parent cells treated with HA 0.01.
$^{\#}P<0.05$ vs Neo1 cells treated with HA 1.
$^{\#\#}P<0.05$ vs Neo2 cells treated with HA 1.
$^{\#\#\#}P<0.05$ vs parent cells treated with HA 1.
$^{+}P<0.05$ vs Neo1 cells treated with HA 0.1.
$^{++}P<0.05$ vs Neo2 cells treated with HA 0.1.
$^{+++}P<0.05$ vs parent cells treated with HA 0.1.

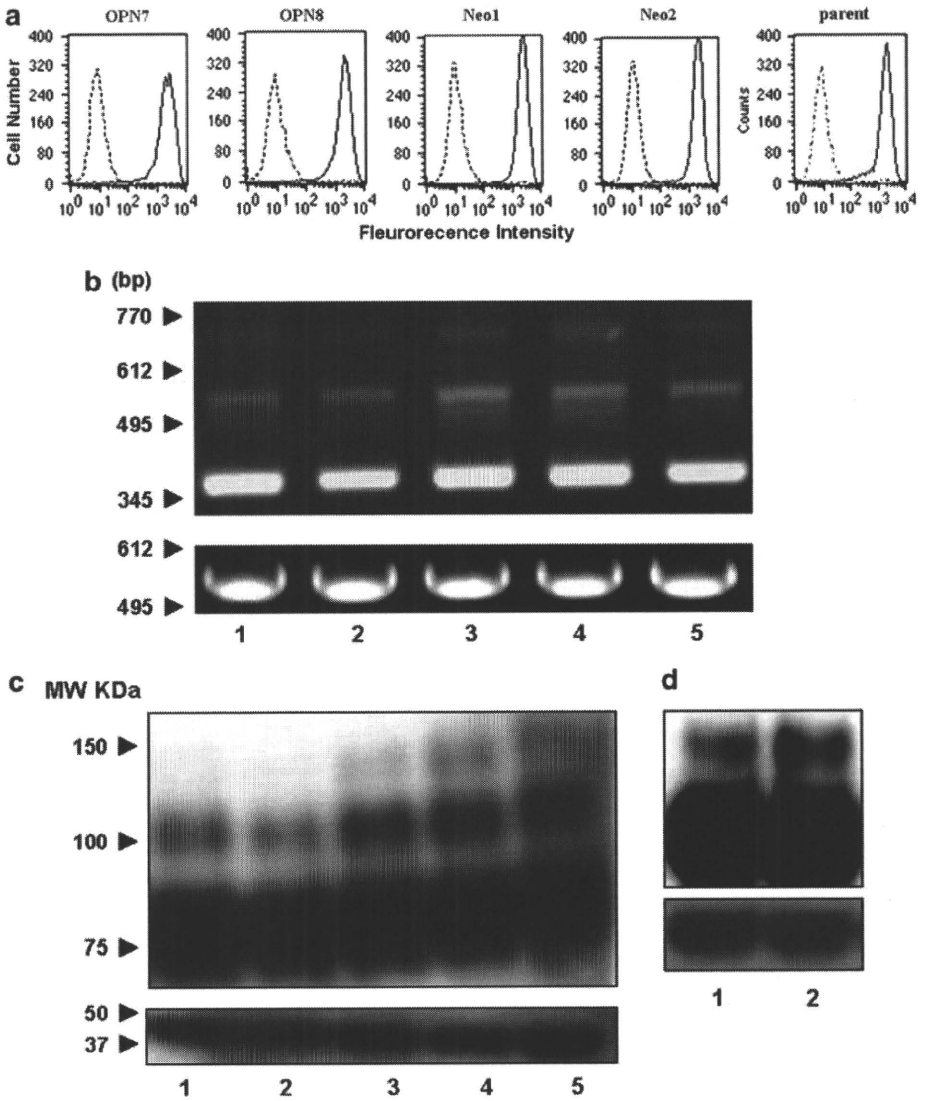

Figure 3 The expression of CD44 and CD44variant forms on ACC-MESO-1/OPN, ACC-MESO-1/Neo and parental cells. (**a**) To determine the CD44 expression, ACC-MESO-1/OPN, ACC-MESO-1/Neo and parental cells were incubated with monoclonal anti-CD44 (BU52, 1 μg/ml) antibody and analyzed with FACScan. (**b**) CD44 mRNA expression by ACC-MESO-1/OPN#7 (lane 1), ACC-MESO-1/OPN#8 (lane 2), ACC-MESO-1/Neo#1 (lane 3), ACC-MESO-1/Neo#2 (lane 4) and ACC-MESO-1 cells (lane 5) were shown. A bottom panel of each set shows β-actin expression as a control. DNA size markers are shown on the left side. (**c**) The expression of CD44s and variants on ACC-MESO-1/OPN#7 (lane 1), ACC-MESO-1/OPN#8 (lane 2), ACC-MESO-1/Neo#1 (lane 3), ACC-MESO-1/Neo#2 (lane 4) and ACC-MESO-1 (lane 5) were assessed by western blotting with anti-CD44 antibody (BU52). A bottom panel shows β-actin expression as loading control. The molecular weight size markers are indicated on the left side. (**d**) The expression of CD44s and variants on ACC-MESO-1 cells cultured on OPN (lane 1) and BSA (lane 2). CD44 protein expression was detected by western blotting. Bottom panel shows β-actin expression as loading control.

reached at any concentration of GEM in the ACC-MESO-1 cells transfected with CD44v10 siRNA, we could not show the IC_{50} against these cells. The IC_{50} of GEM against the cells transfected with control siRNA was $0.08 \pm 0.009\,\mu M$ (Figure 4d). As expected, the silencing of the CD44v10 expression in ACC-MESO-1 cells increases the multidrug resistance. The silencing of CD44v10 expression in ACC-MESO-1 cells also increases adhesion to HA (data not shown). These results suggest that the downregulation of CD44v10, accompanied by the enhanced adhesion to HA, is involved in the multidrug resistance.

Inhibition of the HA–CD44 interaction abrogated multidrug resistance and resistance to apoptosis

To determine whether HA–CD44 interaction is involved in the mechanism of the multidrug resistance, the expression of CD44 in ACC-MESO-1/OPN and ACC-MESO-1/Neo cells were downregulated by siRNA. siRNA transfection downregulated the CD44 expression by >70% and then a chemosensitivity assay was performed (Figure 5a). The IC_{50} of NVB against the OPN8 cells transfected with CD44 siRNA, OPN8 cells transfected with control siRNA, Neo2 cells transfected with CD44 siRNA and Neo2 cells transfected with